

1 Inhibition of the sodium-dependent HCO₃⁻ transporter SLC4A4, produces a cystic fibrosis-like
2 airway disease phenotype.

3 Vinciane Saint-Criq^{1,δ}, Anita Guequén^{2,3}, Amber Philp^{2,3}, Sandra Villanueva², Tábata Apablaza^{2,3},
4 Ignacio Fernández-Moncada², Agustín Mansilla^{2,3}, Livia Delpiano¹, Iván Ruminot^{2,4}, Cristian
5 Carrasco⁵, Michael A. Gray¹, Carlos A. Flores^{2,4}.

6 ¹Biosciences Institute, The Medical School, Newcastle University, Newcastle upon Tyne, United
7 Kingdom

8 ²Centro de Estudios Científicos (CECs), Valdivia, Chile.

9 ³Universidad Austral de Chile, Valdivia, Chile.

10 ⁴Universidad San Sebastián, Chile.

11 ⁵Subdepartamento de Anatomía Patológica, Hospital Base de Valdivia, Valdivia 5090000, Chile.

12
13 ^δCurrent affiliation: Université Paris-Saclay, INRAE, AgroParisTech, Micalis Institute, 78350, Jouy-
14 en-Josas, France

15
16 Corresponding author:

17 Carlos A. Flores. cflores@cecs.cl

18

19 ABSTRACT

20 Bicarbonate secretion is a fundamental process involved in maintaining acid-base homeostasis.
21 Disruption of bicarbonate entry into airway lumen, as has been observed in cystic fibrosis,
22 produces several defects in lung function due to thick mucus accumulation. Bicarbonate is critical
23 for correct mucin deployment and there is increasing interest in understanding its role in airway
24 physiology, particularly in the initiation of lung disease in children affected by cystic fibrosis, in the
25 absence of detectable bacterial infection. The current model of anion secretion in mammalian
26 airways consists of CFTR and TMEM16A as apical anion exit channels, with limited capacity for
27 bicarbonate transport compared to chloride. However, both channels can couple to SLC26A4
28 anion exchanger to maximise bicarbonate secretion. Nevertheless, current models lack any details
29 about the identity of the basolateral protein(s) responsible for bicarbonate uptake into airway
30 epithelial cells. We report herein that the electrogenic, sodium-dependent, bicarbonate
31 cotransporter, SLC4A4, is expressed in the basolateral membrane of human and mouse airways,
32 and that its pharmacological inhibition or genetic silencing reduces bicarbonate secretion. In fully
33 differentiated primary human airway cells cultures, SLC4A4 inhibition induced an acidification of
34 the airways surface liquid and markedly reduced the capacity of cells to recover from an acid load.
35 Studies in the *Slc4a4*-null mice revealed a previously unreported lung phenotype, characterized by
36 mucus accumulation and reduced mucociliary clearance. Collectively, our results demonstrate that
37 the reduction of SLC4A4 function induced a CF-like phenotype, even when chloride secretion
38 remained intact, highlighting the important role SLC4A4 plays in bicarbonate secretion and
39 mammalian airway function.

INTRODUCTION.

Bicarbonate (HCO_3^-) and chloride (Cl^-) are actively secreted into the lumen of airways by the lining epithelial cells. Even though, the pathophysiological consequences of decreased secretion of these anions has been extensively documented in cystic fibrosis (CF), the most common, autosomal recessive, disease in humans, there is still much discussion whether HCO_3^- secretion *per se* affects airway homeostasis (1, 2). Impaired Cl^- secretion reduces the volume of the fluid that covers the airway epithelium, the airway surface liquid (ASL), leading to ciliary dysfunction and promoting mucus stasis and airway obstruction (3, 4). Deficient HCO_3^- secretion reduces ASL pH which compromises post-secretory mucin maturation and clearance (5), impairs the antimicrobial function of epithelial cells (6, 7) and increases fluid absorption, further decreasing ASL hydration (8). Whilst, direct measurement of pH in the distal airways of CF children showed no acidification of the ASL (9), it has been demonstrated that the addition of HCO_3^- induced an increase in ASL height in human airway epithelial cells (hAECs) cultures and restored the normal properties of mucus from CF patients (8, 10). Moreover, the use of aerosolized HCO_3^- into CF-pig airways increased bacterial killing, clearly indicating that HCO_3^- supplementation can correct inherent defects of CF in the airways (6, 11).

Even though, impaired HCO_3^- secretion is recognised as a detrimental component of CF airway disease, a full mechanistic understanding of the process and players involved in transcellular HCO_3^- transport in the airways is lacking. In normal airways, HCO_3^- is secreted by CFTR and TMEM16A channels, but after inflammatory signalling, HCO_3^- secretion is augmented through increased expression of the $\text{Cl}^-/\text{HCO}_3^-$ exchanger Pendrin (SLC26A4) (12–16). Importantly, the mechanism of basolateral HCO_3^- transport/uptake in native pulmonary tissues is still lacking. We reasoned that the identification and functional inhibition of such basolateral membrane proteins could be used

as a proof-of-concept to better understand the role of HCO_3^- secretion in airway homeostasis without altering Cl^- secretion. Here using *in vitro* fully differentiated human bronchial epithelial cells, we identified the Na^+ -dependent, HCO_3^- electrogenic cotransporter (NBCe1), SLC4A4, as the basolateral protein responsible for HCO_3^- influx, which couples to apical CFTR for HCO_3^- secretion into the ASL. Importantly, SLC4A4 inhibition induced acidification of the ASL, revealing the pivotal role of this cotransporter in airway pH homeostasis. These observations were further tested in murine models, and revealed that SLC4A4 is involved in both basal and Ca^{2+} -stimulated HCO_3^- secretion in mice airways. Strikingly, an *Slc4a4*^{-/-} mouse model showed significant pathological signs of muco-obstructive disease and reduced mucociliary clearance, confirming that inhibition of HCO_3^- secretion alters airway homeostasis, mimicking what has been observed in human CF, and identifying a critical role played by SLC4A4.

75 RESULTS

76 **Primary human airway epithelial cells express bicarbonate transporters of the SLC4A family.**

77 We first investigated, by PCR, whether primary hAECs expressed different members of the SLC4A
78 family of Na^+ -coupled HCO_3^- transporters (NCBT) and isolated RNA from kidney and the Calu-3 cell
79 line, which was derived from a metastatic site of a lung adenocarcinoma, as positive controls. The
80 use of specific primers (Supplementary File 1) for each NCBT revealed that *SLC4A4*, *SLC4A5*,
81 *SLC4A7* and *SLC4A8* are expressed at mRNA levels in primary hAECs from 3 different individuals
82 (P1, P2, P3, Figure 1- figure supplement 1A-E). *SLC4A10* showed near undetectable level of mRNA
83 expression (Figure 1-figure supplement 1F). Interestingly, isoforms B/C of NBCe1 (known as the
84 pancreatic isoform, Figure 1-figure supplement 1A) were more highly expressed than isoform A
85 (known as the kidney isoform; Figure 1- figure supplement 1E). Data extraction from previously
86 published RNA-seq results (17) (GEO series accession number GSE154905) confirmed the pattern
87 of expression of these isoforms (Figure 1-figure supplement 1G) and revealed that *SLC4A4* is the
88 most expressed member, closely followed by *SLC4A7*, *SLC4A8* and *SLC4A5*. Other candidate HCO_3^- -
89 transporters such as Bestrophins were also expressed in these cells but with one to two logs lower
90 than *SLC4A4*, *SLC4A7* and *SLC4A8* (Figure 1-figure supplement 1G).

91 **SLC4A4 is central for bicarbonate secretion and intracellular pH homeostasis in human airway** 92 **cells.**

93 We then tested whether there was an active NCBT under unstimulated and stimulated conditions
94 in primary hAECs. The cell cultures were mounted in Ussing chambers in buffers containing either
95 HCO_3^- (but no Cl^-) or HEPES (no HCO_3^-), and treated basolaterally with the inhibitor S0859 (30 μM)
96 followed by Forskolin (Fsk; 10 μM). Results, shown in Figure 1 confirmed that, in the absence of
97 stimulants, HCO_3^- secretion was inhibited by S0859 (Figure 1A,B) and that this pharmacological

inhibitor did not have any effect on short-circuit current (I_{sc}) in the absence of HCO_3^- (Figure 1D,E). Interestingly, S0859 did not reduce Fsk-stimulated HCO_3^- secretion (Figure 1C) under these conditions. These results show that there is an electrogenic HCO_3^- transporter at the basolateral membrane of hAECs, which is consistent with SLC4A4, since SLC4A7 and SLC4A8 are electroneutral (18), and SLC4A5 has been shown to be localized to the apical membrane of renal epithelial cells and cholangiocytes (19, 20). Next, we used intracellular pH (pH_i) measurements to functionally investigate NBCe1 activity using a CO_2 -induced acidification protocol (21). As shown in Figure 1E, exposing cells bilaterally to a $\text{HCO}_3^-/\text{CO}_2$ -gassed KRB solution induced a transient acidification. On the other hand, an apical-only CO_2 exposure, in the absence of basolateral HCO_3^- , induced a sustained acidification (of the same amplitude as with bilateral $\text{HCO}_3^-/\text{CO}_2$, Figure 1F,H), that recovered when HCO_3^- was re-introduced basolaterally (Figure 1F,I). This pH_i recovery depended on the presence of Na^+ in the basolateral solution (Figure 1G) consistent with a Na^+ -coupled HCO_3^- transporter, which was confirmed using S0859 which blocked the pH_i recovery from the CO_2 -induced acidification. In order to isolate NBCe1-dependent changes in pH_i , the contribution of Na^+/H^+ exchanger NHE was inhibited using 100 μM Dimethyl amiloride (DMA). In this condition, S0859 still significantly decreased the rate of pH_i recovery from the CO_2 -induced acidification (Figure 1J,K).

Basolateral HCO_3^- uptake is essential for ASL pH homeostasis.

As Ussing chamber and pH_i experiments use standard buffer solutions that are unlikely to fully resemble that of the ASL, we then used fully differentiated hAECs at the air-liquid interface to establish whether SLC4A4 is involved in airway epithelial pH homeostasis in a setting that is more physiologically relevant. In order to test whether HCO_3^- transport by basolateral SLC4A4 impacted apical HCO_3^- secretion under thin film conditions, we measured the effect of S0859 on ASL pH.

First, S0859 was added basolaterally to primary hAECs and ASL pH continuously measured. NBCe1 inhibition significantly decreased ASL pH under resting conditions with a $t_{1/2}$ of 46 min (Figure 2A,B), and partially prevented the Fsk-induced increase in ASL pH which we have previously shown was via CFTR (22, 23)(Figure 2C,D), increasing the half-time response to Fsk from 25 to 31 min. Moreover, when S0859 was added after Fsk, it significantly reduced the Fsk-induced, CFTR-dependent, increase in ASL pH with a half-time of 14 min (Figure 2E,F) confirming the central role of SLC4A4 cotransporter in ASL pH homeostasis under both resting and stimulated conditions. It is worth noting that the changes in ASL pH were much slower than in the pH_i experiments, which can be explained by the differences in technical (non-perfused ASL pH versus bilaterally perfused pH_i) and experimental conditions set-ups (chemical induced versus. CO_2 induced changes in pH).

Finally, immunolocalization of SLC4A4 protein in human airway tissues showed intracellular and basolateral membrane staining in epithelial cells that were also positively stained for acetylated-tubulin indicating that SLC4A4 is preferentially expressed in ciliated cells in human airways (Figure 2G,H).

Bicarbonate secretion is calcium-activated in mouse trachea.

To investigate the expression of SLC4 exchangers in mouse airway epithelium, we performed RT-PCR of epithelial cells from mouse tracheas and observed that several members of the SLC4 family including *Slc4a4*, *Slc4a5*, *Slc4a7* and *Slc4a10* were expressed (Figure 3-supplemental figure 1A-E). Studies of *Slc4a4* isoforms demonstrated that isoform B/C but not isoform A was expressed in mouse airways (Figure 3- figure supplement 1F). Next we characterized HCO_3^- secretion in the mouse. Using chamber experiments performed in freshly excised mouse trachea using HCO_3^- (Figure 3A) or HEPES (Figure 3B) buffered solutions, showed that UTP-induced an anion current that was significantly reduced in the absence of HCO_3^- (-138 ± 28 vs $-82 \pm 15 \mu A cm^{-2}$; $p < 0.01$

Mann-Whitney test), but no significant effect on the cAMP-induced anion secretion, or the amiloride-sensitive sodium absorption (Figure 3C) was detected as previously shown (24). Complementary studies in HCO_3^- buffer showed that *de novo* synthesis of HCO_3^- was not participating in the UTP-induced electrogenic anion secretion, as incubation of tracheas with acetazolamide didn't affect the magnitude of the UTP-induced current ($-124 \pm 14 \mu\text{A cm}^{-2}$; $p > 0.05$ One-way ANOVA).

Using the SLC4A4 blocker S0859, we observed the inhibition of the cAMP-induced anion current ($\Delta I_{sc} -12.2 \pm 2.4 \mu\text{A cm}^{-2}$) suggesting that SLC4A4 might participate in the cAMP-response (Figure 3- figure supplement 2A-C). Nevertheless, when the TMEM16A/CFTR inhibitor, CaCCinhA01, was used to block the cAMP-induced current, further addition of S0859 was still able to induce a reduction in the current and of similar magnitude as shown in Figure 3- figure supplement 2A (Figure 3- figure supplement 2D-F; $-10.1 \pm 2.8 \mu\text{A cm}^{-2}$), confirming that electrogenic-bicarbonate secretion was not significantly stimulated by cAMP, indicating that basal HCO_3^- secretion occurs in mouse trachea. To confirm this last hypothesis we added S0589 to tissues pre-incubated with amiloride and observed a reduction in the basal current only in HCO_3^- buffer (-13.9 ± 3.3 vs $-3.0 \pm 1.6 \mu\text{A cm}^{-2}$ for HCO_3^- vs HEPES buffer; $p < 0.02$; Mann-Whitney; Figure 3D-F). The magnitude of basal HCO_3^- secretion inhibited by S0859 was similar to the experiments summarized in Figure 3- figure supplement 2C and 2F. Of note, the addition of S0859 to the tracheas induced a fast and transient negative change in I_{sc} as observed in Figure 3D and E and Figure 3- figure supplement 2A and D, that has been also observed in human cells (25), and that might be due to off-targets of the blocker like other SLC4A or SLC16A transporters as previously described (26–28).

To further characterize the Ca^{2+} -activated anion secretion, the UTP response was tested with no involvement of cAMP-induced secretion. As can be observed (Figure 3G,H) the UTP-induced anion

secretion in tracheas maintained in HCO_3^- buffer was significantly reduced by previous addition of S0859 (-368 ± 25 vs $-200 \pm 17 \mu\text{A cm}^{-2}$; $p < 0.001$ One-way ANOVA). The UTP response was also reduced when HCO_3^- was replaced with HEPES buffer (Figure 3I) ($-199 \pm 25 \mu\text{A cm}^{-2}$; $p < 0.001$ One-way ANOVA), but the addition of S0859 induced no significant reduction of the UTP-induced anion secretion in tissues maintained in HEPES buffer (Figure 3J) ($-142 \pm 12 \mu\text{A cm}^{-2}$; $p > 0.05$ One-way ANOVA).

SLC4A4 participates in intracellular pH homeostasis in mouse airway epithelial cells.

We reasoned that the UTP-induced HCO_3^- exit would lead to cytoplasmic acidification and therefore we monitored intracellular pH of BCECF-loaded murine airway cells. As shown in Figure 3L, UTP induced an intracellular acidification ($\Delta\text{pH}_i -0.25 \pm 0.02$) that was significantly reduced when cells were placed in low Cl^- buffer ($\Delta\text{pH}_i -0.11 \pm 0.02$), indicating the existence of $\text{Cl}^-/\text{HCO}_3^-$ exchange. Figure 3M summarizes changes in intracellular pH and includes experiments in HEPES buffer, which shows that UTP was almost unable to induce intracellular acidification ($\Delta\text{pH}_i -0.01 \pm 0.01$) in absence of HCO_3^- . To test if the UTP-induced intracellular acidification was dependent on SLC4A4 activity, we tested the S0859 inhibitor and observed acidification of the intracellular compartment and prevention of UTP-induced acidification (Figure 3- figure supplement 2G-H). Washout of S0859 partially restored pH_i and UTP-induced acidification. (Figure 3-figure supplement 2G-H; -0.05 ± 0.01 vs $-0.13 \pm 0.03 \Delta\text{pH}_i$, for UTP with S0559 and UTP post washout respectively; $p > 0.002$; Mann-Whitney). These data suggest that both basal and UTP-induced HCO_3^- secretion are dependent on SLC4A4 activity in mouse airway epithelial cells.

The genetic inactivation of *Slc4a4* induces a cystic fibrosis-like phenotype in mouse airways.

As explained in the methods section, we decided to work with wild type and *Slc4a4*^{-/-} on the hybrid background, at 16-20 days of age. First, we observed that *Slc4a4*^{-/-} animals were affected by

defects in tracheal cartilage formation with the presence of ventral gaps and abnormal patterns on the rostrocaudal side (Figure 4A). In wild type animals, immunolocalization of SLC4A4 showed strong localization in the airway epithelium but the signal was nearly absent in the airways from the *Slc4a4*^{-/-} mice (Figure 4B). Using the same antibody, we showed that SLC4A4 was preferentially expressed in CCSP-positive cells that correspond to Club cells and was excluded from cells positive to acetylated-Tubulin, that identify ciliated cells (Figure 4C). This pattern of expression was maintained in distal airway bronchi and bronchioles (Figure 4- figure supplement 1C). Further histological examination of the *Slc4a4*^{-/-} mouse airways demonstrated the presence of adherent mucus at the surface of the tracheal epithelium (Figure 4D and Figure 4- figure supplement 1C,D) as well as in the bronchi (Figure 4-figure supplement 1E-G) and bronchioli (Figure 4- figure supplement 1H). Signs of damaged epithelium was also observed as interruptions in the epithelial layer facing the lumen in the *Slc4a4*^{-/-} airways (Figure 4D and Figure 4- figure supplement 1F,H), that might explain the decreased R_{te} of the tracheas placed in Ussing chambers and that prevented electrophysiological measurements in the *Slc4a4*^{-/-} tracheas (Figure 4E).

Genetic silencing of *Slc4a4* impairs intracellular pH homeostasis and mucociliary clearance in mouse airways.

In order to validate the role of SLC4A4 in pH homeostasis of murine airways, UTP-induced intracellular acidification was studied in airway cells isolated from the *Slc4a4*^{-/-} mice. We observed a decrease in the magnitude of intracellular acidification in *Slc4a4*^{-/-} cells when compared to those from wild type animals during UTP stimulation (-0.24 ± 0.01 vs -0.14 ± 0.01 $\Delta pH_{[i]}$, for wild type vs *Slc4a4*^{-/-}) suggesting that an important amount of HCO_3^- accumulates in airways cells via SLC4A4 (Figure 4F-G). We also noticed that after UTP wash-out, the acidification persisted in the wild type cells but not in the *Slc4a4*^{-/-} (Figure 4- figure supplement 1J; -0.09 ± 0.02 vs -0.02 ± 0.01 $\Delta pH_{[i]}$, for

wild type vs *Slc4a4*^{-/-}), suggesting that HCO₃⁻ secretion was sustained by SLC4A4 activity. Clearance of plastic beads, as a way to measure MCC, was studied in freshly isolated mouse tracheas whose mucosal side was exposed to air. As shown in the polar plots in Figure 4H the plastic beads covered a larger distance in wild type tissues and, in some cases, retrograde movement of beads was observed in the *Slc4a4*^{-/-} trachea. A similar reduction in distance travelled was observed in wild type tissues bathed in HEPES buffer. The speed of plastic bead movement and total distance covered are summarized in Figure 4I,H. The use of HEPES buffer in the *Slc4a4*^{-/-} tracheas showed no further effect on both speed and total distance travelled by the beads. This data set demonstrates that mucociliary clearance is significantly decreased when HCO₃⁻ transport is impaired after *Slc4a4* silencing.

223

DISCUSSION

SLC4A4 is a critical component of the bicarbonate secretory machinery.

In this study we have established that the Na^+ -coupled HCO_3^- transporter SLC4A4 or NBCe1 is central for bicarbonate transport, coupling to apical proteins to efficiently deliver bicarbonate in human and mouse airways. As the specificity of S0859 for SLC4A4 has been discussed and is still unclear (26–28), it is uncertain from our data whether SLC4A4 is the main and only actor regulating bicarbonate uptake in primary hAECs. However its importance in airway pH homeostasis is supported by strong evidence from the use of knock-out animals. Early characterization in canine and human airway epithelium indicated that HCO_3^- secretion occurs via CFTR, is activated by cAMP and dependent on basolateral Na^+ (29), similar features were observed in the Calu-3 cell line (30). Our experiments in hAECs corroborated the cAMP-activation and Na^+ -dependence, that has also been observed by others in the same (14, 25) or other cell types (31). Nevertheless, and in contrast to human airway epithelium, our present data shows that HCO_3^- secretion in the mouse airways is mostly Ca^{+2} - rather than cAMP-activated, but both human and mouse share a basal secretory component for HCO_3^- previously observed in human bronchioles (32), and that we now show is dependent on SLC4A4 activity.

Basolateral localization of SLC4A4 was previously demonstrated in the Calu-3 cell line (33) but up to the date there has been no other studies investigating SLC4A4 localization in native airway tissues. Here we demonstrate that human airways express SLC4A4 in ciliated cells preferentially, and that the observed basolateral localization correlates with the functional evidence provided, reinforcing the role SLC4A4 in basolateral HCO_3^- transport into the cells. Nevertheless, it must be considered that the sole expression of SLC4A4 does not assure HCO_3^- secretion as compelling evidence has demonstrated that apical CFTR is also necessary. While the calcium-activated

TMEM16A channel has been shown to be expressed in goblet cells (34), both HCO_3^- transporters, CFTR and pendrin, have been localized in the apical membrane of ciliated hAECs cells supporting our observation (14, 35). Moreover, it has been demonstrated that SLC4A4-B, that we detected in human and mouse, and not the isoform A, is functionally coupled to CFTR through the IRBIT protein in pancreatic ducts (36, 37), further supporting the idea that a functional coupling in the same cell type is necessary for efficient HCO_3^- secretion. Even though, CFTR and Pendrin expression increases in secretory cells after cytokine stimulation, SLC4A4 remained unaltered, suggesting that other basolateral HCO_3^- transporter support HCO_3^- secretion in human secretory cells during the inflammatory response (15). Finally, CFTR distribution in airway epithelium has been under renewed scrutiny after the recent discovery of the pulmonary ionocyte, a rare airway epithelial cell type that contains the highest amount of *CFTR/Cftr* transcripts in human and mouse (38, 39). Nevertheless, recent and detailed studies demonstrate that most human airway epithelial cell types express CFTR including ciliated cells as was initially demonstrated (40, 41).

We noticed that SLC4A4 localization in mouse was different from human airway epithelium, as the mouse SLC4A4 was expressed in CCSP+ and not ciliated cells. Previously, CFTR and TMEM16A channels were specifically located in non-ciliated cells of mouse airways (42), a distribution also conserved in the rat (43). Pendrin, was also detected in non-ciliated secretory MUC5AC+ cells, suggesting that a functional coupling for HCO_3^- secretion occurs in secretory non-ciliated cells of the mouse airways (44). Such a difference in expression of transporter proteins among human and mouse airways has frequently been described; for example CFTR, is not the principal Cl^- transporter in the mouse airways and consequently silencing or mutation of *Cftr* in mice did not produce CF disease of the lungs (45, 46). Furthermore, the expression in human and not mouse airways of another protein that influence ASL pH, the ATP12A H^+/K^+ ATPase, magnifies ASL acidification in human airways in CF disease (7).

Impaired bicarbonate secretion produces a CF-like phenotype in the mouse airways. We demonstrated that SLC4A4 activity is pivotal for HCO_3^- secretion. Inhibition of SLC4A4 induced acidification of the ASL in hAECs, an observation that suggests altering HCO_3^- delivery can initiate a CF-like phenotype, and that was confirmed in the *Slc4a4*^{-/-} mouse model. Previous observations obtained by inducing silencing of *Tmem16a* in the mouse, or using cells carrying natural mutations in CFTR, affected both Cl^- and HCO_3^- secretion making it difficult to understand what the consequences of reduced transport for each anion alone are (25, 47). As observed here, the silencing of *Slc4a4* induced a muco-obstructive phenotype in the mouse, whereas the silencing of *Slc12a2*, which encodes the bumetanide-sensitive NKCC1 co-transporter, which is essential for Cl^- accumulation and secretion, did not (48), suggesting that lack of HCO_3^- is pathologically more relevant than Cl^- secretion in mouse airways. Indeed, a significant amount of experimental evidence, using different models and species, is consistent with our findings in the *Slc4a4*^{-/-} mouse. For example, hAEC from CF patients produce acidic ASL and mucus that is more viscous than in cells from non-CF donors (49), the acidification of the ASL induced abnormal epithelial immune responses and reduced MCC that could be reversed after HCO_3^- supplementation (6, 7, 50–53). Furthermore, HCO_3^- secretion is necessary for proper mucus release from hAECs (25), and maintenance of normal amounts of ENaC-mediated Na^+ absorption and ASL volume (8), functions that become abnormal due to acidic ASL pH. Even though technically challenging issues prevented us from measuring ASL pH in the mouse trachea, the reduction of HCO_3^- transport demonstrated here after SLC4A4 inhibition is consistent with the expected muco-obstructive phenotype, including reduced MCC and mucus accumulation.

Extra-renal phenotypes after *Slc4a4* inactivation and human mutations.

Mouse models of *Slc4a4* silencing have shown differences in phenotypes depending on the isoforms affected. The *Slc4a4*-null animal, corresponding to the one used in the present studies, and the *Slc4a4*^{W516X/W516X} avatar mouse engineered to mimic a non-sense mutation found in a human patient, are affected by severe metabolic acidosis due to proximal renal tubular acidosis (pRTA)(54, 55). Even though, decreased plasma HCO₃⁻ is observed in the *Slc4a4*^{-/-} mice (5.3 ± 0.5 mM) (54), is unlikely that reduced HCO₃⁻ availability influenced mucus accumulation in the airways, as we have previously determined that the transporter is fully saturated at 3 mM HCO₃⁻ (56).

Extra-renal manifestations of *Slc4a4* silencing in the mouse include growth retardation, ocular band keratopathy, splenomegaly, abnormal dentition and intestinal obstructions, most of which mimics the clinical findings observed in human patients. Nevertheless lung defects have not been reported in human patients, and observation which could be explained by the fact that human disease is milder than in mouse models. This might be related to the fact that at birth human kidneys are functionally more mature than in mouse (57) and for example, while heterozygous animals present mild pRTA, human patients bearing heterozygous SLC4A4 mutations did not show any signs of disease (54, 55). Even though, a compensatory activity of other Na⁺-coupled HCO₃⁻ cotransporters, or exchangers, has been discarded in mouse, this possibility has not been examined in humans where compensatory activity might benefit patient's health (55).

Both the *Slc4a4*^{-/-} and W516X-mutant animals die soon after weaning as we also observed, but while the specific knock-out mouse for SLC4A4 isoform A (NBCe1-A) has a normal life span, the knock-out mouse for SLC4A4 isoforms B and C (NBCe1-B/C) is still lethal. This suggests that the cause of death of the animals was not due to metabolic acidosis, but rather due to extra renal phenotypes worsened by pRTA (58, 59). This observation might also be linked to the influence of modifier genes as observed in human patients and CF mouse models (60–62). In this regard, our

316 observation that lethality is dependent on the genetic background of the animals supports such a
317 possibility.

318 It will be of interest to use the *Slc4a4* animal models and generate an airway specific null mouse to
319 study the pathogenesis of muco-obstructive diseases of the lungs due to reduced HCO_3^- secretion.

320 We believe that the elucidation of the transport systems that participate in pH maintenance in the
321 airways offers the chance of increasing our current knowledge of the impact of impaired
322 bicarbonate transport during health and disease.

323

METHODS

***In vitro* Human airway epithelial cells studies**

Cell culture. Primary hAECs were a kind gift from Dr. Scott H. Randell (Marsico Lung Institute, The University of North Carolina at Chapel Hill, United States). The cells were obtained under protocol #03-1396 approved by the University of North Carolina at Chapel Hill Biomedical Institutional Review Board. Cells were expanded using the conditionally reprogrammed cell (CRC) culture method as previously described (63). Briefly, cells were seeded on 3T3J2 fibroblasts inactivated with mitomycin C (4 mg/ml, 2 h, 37°C) and grown in medium containing the ROCK inhibitor Y-27632 (10 mM, Tocris Biotechne, #1254) until they reached 80% confluence. Cells then underwent double trypsinization to remove the fibroblasts first and then detach the hAECs from the P150 dish. At that stage, cells were counted and could be frozen down. Cryopreserved cells were seeded onto semi-permeable supports (6.5 or 12 mm) in bilateral differentiating medium (ALI medium) as previously described (64). The apical medium was removed after 3-4 days and cells were then allowed to differentiate under air-liquid interface (ALI) conditions. Ciliogenesis started approximately 12–15 days after seeding and cells were used for experiments between days 25 and 35 after seeding.

Intracellular pH measurements. Primary airway epithelial cells, grown on 12 mm Transwell inserts, were loaded with the pH-sensitive, fluorescent dye BCECF-AM (10 μ M, ThermoFisher Scientific #B-1150) for 1h in a Na-HEPES buffered solution (130 mM NaCl, 5 mM KCl, 1 mM MgCl₂, 1 mM CaCl₂, 10 mM Na-HEPES, and 5 mM D-glucose set to pH 7.4) at 37°C. Cells were mounted on to the stage of a Nikon fluor inverted microscope and perfused with a modified Krebs (KRB) solution (115 mM NaCl, 5 mM KCl, 25 mM NaHCO₃, 1 mM MgCl₂, 1 mM CaCl₂, and 5 mM D-glucose) gassed with 5% (v/v) CO₂/95% (v/v) O₂ or with a Na-HEPES-buffered solution gassed with

100% O₂. Solutions were perfused across the apical and basolateral membranes at 37°C at a speed of 3 ml min⁻¹ and 6 ml min⁻¹, respectively. To test the sodium dependence of bicarbonate transport, a Na⁺-free KRB solution was used in which 115 mM NMDG-Cl replaced NaCl, and 25 mM choline-HCO₃ replaced NaHCO₃. To measure the effect of NBC inhibition on the recovery from CO₂-induced acidification, epithelial cells were perfused basolaterally with 100 μM DMA (dimethyl amiloride, Sigma-Aldrich #A4562) to inhibit sodium-dependent hydrogen exchangers (NHEs) and 30 μM S0859 (Sigma-Aldrich #SML0638) to inhibit NBC. Intracellular pH (pH_i) was measured using a Life Sciences Microfluorimeter System in which cells were alternately excited at 490 and 440 nm wavelengths every 1.024 s with emitted light collected at 510 nm. The ratio of 490 to 440 nm emission was recorded using PhoCal 1.6 b software and calibrated to pH_i using the high K⁺/nigericin technique (65) in which cells were exposed to high K⁺ solutions containing 10 μM nigericin, set to a desired pH, ranging from 6 to 7.5. For analysis of pH_i measurements, ΔpH_i was determined by calculating the mean pH_i over 60 s resulting from treatment. The initial rate of pH_i change (ΔpH_i/Δt) was determined by performing a linear regression over a period of at least 40 s.

Short-Circuit Current Measurements in human airway epithelial cells. Cells grown on 6.5 mm inserts were mounted into the EasyMount Ussing Chamber Systems (VCC MC8 Physiologic Instrument, tissue slider P2302T) and bathed in bilateral Cl⁻ free HCO₃⁻ KRB (25 mM NaHCO₃, 115 mM Nagluconate, 2.5 mM K₂SO₄, 6.0 mM Ca-gluconate, 1 mM Mg-gluconate, 5 mM D-glucose) continuously gassed and stirred with 5% (v/v) CO₂/95% (v/v) O₂ at 37°C or in bilateral NaHEPES buffered solution continuously gassed and stirred with 100% O₂ at 37°C. Monolayers were voltage-clamped to 0 mV and monitored for changes in short-circuit current (ΔI_{sc}) using Ag/AgCl reference electrodes. The transepithelial short-circuit current (I_{sc}) and the Transepithelial electrical resistance (R_{te}, expressed in Ω cm²) were recorded using Ag–AgCl electrodes in 3 M KCl agar bridges, as previously described (66), and the Acquire & Analyze software (Physiologic

Instruments) was used to perform the analysis. Cells were left to equilibrate for a minimum of 10 min before amiloride (10 μ M, apical, Sigma-Aldrich #A7410) and S0859 (30 μ M, basolateral) were added. Results were normalized to an area of 1 cm² and expressed as I_{sc} (μ Amp.cm⁻²). The number of replicates was determined using previously obtained short circuit current measurements.

ASL pH Measurements. ASL pH measurements were performed as previously described (22, 23).

Briefly, cells grown on 6.5 mm transwells were washed apically with modified Krebs solution for 15 min at 37°C, 5% CO₂. The ASL was stained using 3 μ l of a mixture of dextran-coupled pH-sensitive pHrodo Red (0.5 mg/ml, λ_{ex} : 565 nm, λ_{em} : 585 nm; ThermoFisher Scientific, #P10361) and Alexa Fluor® 488 (0.5 mg/ml, λ_{ex} : 495 nm, λ_{em} : 519 nm; ThermoFisher Scientific #D-22910) diluted in glucose-free modified Krebs buffer, overnight at 37°C, 5% CO₂. The next day, fluorescence was recorded, every 5 min, using a temperature and CO₂-controlled plate reader (TECAN SPARK 10M) and forskolin (Tocris Biotechne #1099) and S0859 were added basolaterally at indicated times. The ratio of pHrodo to Alexa Fluor® 488 was converted to pH using a calibration curve obtained by clamping apical and basolateral pH in situ using highly buffered solutions between 5.5 and 8 (22). To prevent inter-experiment variability, the standard curve calibration was performed on each independent experiment. Changes in ASL pH (Δ ASLpH) were calculated by averaging five time points (average pH over 25 min) before and 2hrs after the addition of the molecules (Fsk/S0859). The number of replicates was determined using previously obtained ASL pH data (23). Using Cohen's d, a power analysis showed that the sample size of 9 independent experiments has an 80% power to detect an effect size of 0.35 pH unit, assuming a 5% significance level and a two-sided test (baseline ASL pH = 6.82 \pm 0.25).

RNA extraction and PCR analysis. RNA isolation from cells was performed using PureLink® RNA Mini Kit (Ambion, Life technologies, #12183018A), following the manufacturer's instructions.

Briefly, lysates were mixed with 70 % ethanol and loaded onto a silica-membrane column. Columns were washed with different buffers and total RNA was eluted in DNase and RNase-free water and stored at -80°C until use. DNase treatment was performed on 300 ng RNA prior to Reverse Transcription Polymerase Chain Reaction (RT-PCR) using RNase-free DNase I (Roche, # 04716728001) at 37°C for 10 min. Reaction was then stopped by increasing the temperature to 70°C for 10 min. Complementary DNA (cDNA) was synthesized from total RNA (300 ng) using M-MLV Reverse Transcriptase (Promega, #M1701) as per supplier's protocol (1hr at 37°C followed by 10 min at 70°C). Expression of SLC4A family members was evaluated by PCR using specific primers (Supplementary file 1), in a total volume of 25 µL containing 2 µL cDNA template, 5 µL 5X Q5 reaction buffer, 0.5 µL 10 mM dNTP, 1.25 µL 10 µM of each primer, 0.25 µL Q5 high Fidelity Polymerase (New England Biolabs Inc., M0491), 5 µL 5X Q5 high enhancer (Denaturation, 98°C, 30 sec; (98°C 5 sec, 72°C 30 sec -72°C 20 sec) x35 cycles; Final Extension, 72°C, 2 min. PCR products were loaded onto a SYBR Safe DNA stain (Life Technologies, cat. no. S33102)-containing, 2 % agarose gels in TBE and electrophoresis was ran at 90V for 1.5hr. Amplified products were visualized using LAS-3000 Imaging System (Fuji).

***Ex vivo* murine airway studies**

Animals: The *Slc4a4*^{-/-} mice was obtained from its laboratory of origin(54) and bred in the original 129S6/SvEv/Black Swiss background or C57BL/6J. As observed in Figure 4- figure supplement1A-B animals maintained in the C57BL/6J background were severely affected by weight loss and lethality before weaning (day 21 post birth). Therefore experiments were performed in the hybrid animals. The wild type C57BL/6J mice were from The Jackson Laboratories (USA). Animals were bred and maintained in the Specific Pathogen Free mouse facility of Centro de Estudios Científicos (CECs) with access to food and water ad libitum. 8-12 weeks-old or 16-20 days-old, male or female

mice were used. Unless otherwise stated, all procedures were performed after mice were deeply anesthetized via i.p. injection of 120 mg/kg ketamine and 16 mg/kg xylazine followed by exsanguination. All experimental procedures were approved by the Centro de Estudios Científicos (CECs) Institutional Animal Care and Use Committee (#2015-02) and are in accordance with relevant guidelines and regulations.

Ussing chamber experiments: Tracheae were placed in P2306B of 0.057 cm² (Fig 3A-K and Fig S4A-F) or P2307 of 0.031 cm² (Fig 5E) tissue holders and placed in Ussing chambers (Physiologic Instruments Inc., San Diego, CA, USA). Tissues were bathed with bicarbonate-buffered solution (pH 7.4) of the following composition (in mM): 120 NaCl, 25 NaHCO₃, 3.3 KH₂PO₄, 0.8 K₂HPO₄, 1.2 MgCl₂, 1.2 CaCl₂ or HEPES buffer: 130 NaCl, 5 KCl, 1 MgCl₂, 1 CaCl₂, 10 Na-HEPES (pH adjusted to 7.4 using HCl); supplemented with 10 D-Glucose, gassed with 5% CO₂–95% O₂ (bicarbonate buffer) or 100% O₂ (HEPES buffer) and kept at 37°C. The transepithelial potential difference referred to the serosal side was measured using a VCC MC2 amplifier (Physiologic Instruments Inc.). The short-circuit currents were calculated using the Ohm's law as previously described(67). Briefly electrogenic Na⁺absorption was inhibited using 10 μM amiloride (Sigma #A7410), cAMP-dependent anion secretion was induced using an IBMX+Forskolin mixture of 100 μM IBMX (Sigma #I5879) + 1 μM forskolin (Sigma #F6886), Ca²⁺-dependent anion secretion was induced by 100 μM UTP (Sigma #U6750). Acetazolamide (100 μM) was used to inhibit bicarbonate production (Sigma #A7011), to block SLC4A4 30 μM S0859 was used (kindly donated by Juergen Punter, Sanofi-Aventis, France and dissolved in ethanol), and 30 μM CACC_{inh}A01 (Calbiochem) to inhibit CFTR and TMEM16A channels. The ΔI_{sc} values were calculated by subtracting I_{sc} values before from I_{sc} values after the addition of drugs but UTP induced current was calculated as the area under the curve (A.U.C.) of the first 5 minutes post UTP addition using the Acquire & Analyze 2.3v software.

Tissues with R_{te} values below $50 \Omega\text{cm}^2$ were discarded as they were not suitable for *bona fide* electrophysiological determinations (68).

Airway cells isolation and intracellular pH determinations: Tracheae were incubated with Pronase 25 $\mu\text{g}/\text{ml}$ at 37°C for 30 minutes. Then the trachea was placed in a petri dish with DMEM-F12, and the airway epithelium was dissociated by scrapping with tweezers, the cells were collected and spun at 3000 r.p.m. for 5 minutes at room temperature and the supernatant was removed. The cell pellet was incubated with 500 μl of trypsin 1X at 37°C for 5 minutes and centrifuged at 3000 r.p.m for 5 minutes at room temperature and the supernatant was removed. The airway epithelial cells were resuspended into 150 μl of DMEM-F12 medium supplemented with 10% fetal bovine serum (FBS) and seeded on poly-L-lysine coated 25 mm glass coverslips in 35 mm Petri dishes. Freshly isolated cells from mouse trachea were loaded with 0.5 μM BCECF-AM (ThermoFisher Scientific #B-1170) for 10 min at 37°C . After loading, cells were washed and incubated 30 min in imaging solution (see below) to allow probe de-esterification. Cells were mounted into an open chamber and superfused with a bicarbonate buffer imaging solution of the following composition (in mM): 120 NaCl, 25 NaHCO_3 , 3.3 KH_2PO_4 , 0.8 K_2HPO_4 , 1.2 MgCl_2 , 1.2 CaCl_2 and bubbled with air/5% CO_2 . For experiments without bicarbonate, the same HEPES buffer as in Ussing chamber experiments was used and bubbled with 100% O_2 . In the low chloride bicarbonate buffer, 120 mM NaCl was replaced by 115 mM Na-Gluconate and 5 mM NaCl. Experiments were carried out on an Olympus IX70 inverted microscope equipped with a 40X oil-immersion objective (NA 1.3), a monochromator (Cairn, UK) and a CCD Hamamatsu Orca camera (Hamamatsu, Japan), controlled by Kinetics software. All solutions were superfused at 37°C using an in-line heating system (Warner instruments). BCECF was excited sequentially at 490 nm and 440 nm for 0.05-0.1 s and emission collected at 535/15 nm. The F490/F440 ratio was computed and transformed to pH units by performing a pH-clamp. Briefly, cells were exposed to 5 μM nigericin and 20 $\mu\text{g}/\text{ml}$

gramicidin in a buffer composed of (in mM) 10 HEPES, 129 KCl, 10 NaCl, 1.25 MgCl₂, 1 EGTA, 10 glucose, with pH values ranging between 6.8-7.8 and the observed changes in fluorescence were quantified and used to construct a calibration curve.

Airway cell isolation and RT-PCR: Tracheae were incubated with Pronase 25 µg/ml at 37°C for 30 minutes. Trachea was placed in DMEM-F12 with 10 mM D-glucose and epithelium was isolated by scrapping with tweezers and further homogenized in 250 µl Trizol (Trizol Reagent) and RNA isolated following the manufacturer's instructions. The dried pellet of RNA was resuspended with 35 µl nuclease free water and stored at -80°C. Genomic DNA was removed through DNase treatment. The concentration and integrity of RNA isolation was verified using a NanoDrop spectrophotometer Maestrogen. RNA was reverse transcribed into cDNA using the ImProm-IITM Reverse Transcription System (Promega) following manufacturer's recommendations. The specific primer pairs used for *Slc4a4*, *Slc4a5*, *Slc4a7*, *Slc4a8*, *Slc4a10*, *Slc4a4-A* and *Slc4a4-B* PCR amplification are provided in Supplementary file 2. PCR amplification was performed starting with 3-minute template denaturation step at 95°C, followed by 40 cycles of denaturation at 95°C for 30 seconds and combined primer annealing/extension at temperature as appropriate.

Histology and immuno fluorescence: Human tissues were obtained from the Pathological Anatomy Subdepartment of Hospital Base Valdivia (Valdivia, Chile) and corresponded to surgical resections of lung tumors that contained normal parenchyma including epithelium. The studies were approved by the Comité Ético Científico of the Servicio de Salud Los Ríos (CEC-SSV 443-2021). To obtain mice tissues the animals were placed in a 1-litre induction chamber under 1000 ml min⁻¹ flow of air containing 2.5% isoflurane. Then kept under anaesthesia with 2% isoflurane at a constant flow rate of 500 ml min⁻¹ using a mask. Mice were euthanized by exsanguination by severing the inferior vena cava under deep anaesthesia. Mice were perfused with 4%

paraformaldehyde (PFA). Trachea and lung were removed and incubated overnight in 4% PFA at 4°C. Paraffin sections (4 µm) were treated with Trilogy™ 1X (Cell Marque cat# 920P-06), blocked with 2.5% normal goat serum (Vector Laboratories cat# S-1012), and incubated with 1:100 anti-NBCe1 (anti SLC4A4; Alomone cat#ANT-075) 4°C overnight. Sections were incubated with secondary antibody 1:2,000 anti-rabbit Alexa Fluor 488 (Invitrogen cat# A-11008) 2h at room temperature. For colocalization 1:100 anti-NBCe1 was incubated with 1:1,000 anti-Clara Cell Secretory Protein (CCSP; Merck Millipore cat#07-623) or 1:200 anti- alpha tubulin (Santa Cruz cat#sc-5286) overnight at 4°C, and incubated with secondary antibody 1:2,000 anti-rabbit Alexa Fluor 568 (Life Technologies cat#A-11011 or 1:2,000 anti-mouse Alexa Fluor 568 (Life Technologies cat#A-11004) respectively. Nuclei were stained with 1:2,000 propidium iodide (Invitrogen cat#P21493). All immunofluorescence images were captured using a confocal microscope (Olympus FV1000).

Whole-mount trachea Alcian blue cartilage staining: Tissue was fixed in 95% ethanol overnight followed by 2h staining with 0.03% Alcian blue (Sigma cat#A5268) dissolved in 80% ethanol and 20% acetic acid. Samples were cleared in 2% KOH, and pictures taken under a stereomicroscope.

Mucociliary clearance determination: Speed of polystyrene beads in trachea samples was determined as previously described(67). Briefly, the tracheas were isolated and mounted with insert needles onto extra thick blot paper (Bio-Rad) and transferred into a water-saturated chamber at 37°C. The filter paper was perfused with HCO₃⁻ buffered solution of the following composition (in mM): 120 NaCl, 25 NaHCO₃, 3.3 KH₂PO₄, 0.8 K₂HPO₄, 1.2 MgCl₂, 1.2 CaCl₂ (gassed with 5% (v/v) CO₂/95% (v/v) O₂ to maintain solution pH close to 7.4) at a rate of 1 ml min⁻¹ and at 37°C. Polystyrene black dyed microspheres (diameter 6µm, 2.6% solid-latex, Polybead, Polyscience Inc) were washed and resuspended in HCO₃⁻ or HEPES solution and 4 µl of particle solution with

0.3% latex were added onto the mucosal surface of the trachea. Particle transport was visualized every 5 seconds for 15 min using a ZEISS SteREO Discovery.V12, with digital camera Motic (Moticam 5.0). Particle speed was calculated with NIH ImageJ software and speed of MCC was expressed in $\mu\text{m}/\text{sec}$. To inhibit HCO_3^- secretion, HCO_3^- solution was substituted for the HCO_3^- free solution (HEPES) of the following composition (in mM): 145 NaCl, 1.6 K_2HPO_4 , 0.4 KH_2PO_4 , 1.0 MgCl_2 , 1.3 CaCl_2 throughout the experiments. In these experiments, the HCO_3^- free solution (HEPES) was gassed with 100% O_2 gas to maintain solution pH close to 7.4. Beads tracked on each tissue were averaged and were used as corresponding to one tissue sample.

Statistical analysis: Experiments in human cells were analysed using GraphPad Prism v9. Statistical analysis was performed taking into account the number n of independent repetitions (done in different days) of the experiments (stated in the Figure legends) using cells at different passage numbers from 3 different donors. Thus n numbers given in the figure legends are considered as biological replicates. Statistical tests used are indicated in the figure legends and p-values are shown in the figures. Experiments using animals were analysed using the Sigmaplot 12 software. Statistical analysis was performed considering as n the number of animals used as source for tissues. These n numbers given on figure legends are considered biological replicates. For pH_i experiments isolated cells were from at least 3 different animals per group and statistical analysis was performed using values from individual cells. ANOVA on Ranks was used for comparisons of more than 2 data sets while Rank Sum test for comparison of data with 2 data sets. For survival analysis Log Rank test was used. P-value of <0.05 was considered statistically significant. Sample size for experiments in human cells were calculated using Cohen's d, a power analysis showed that the sample size of 5 independent experiments has a 90% power to detect a difference, assuming a 5% significance level and a two-sided test. Calculations were based in previously published data for intracellular pH (65), ASL pH measurements (23) and unpublished data set for short-circuit

534 currents. Sample size for animal experiments was calculated using previous published data for
535 Ussing chamber experiments (67, 68), intracellular pH (69) and mucociliary clearance (67).

536 **Data availability:** All data analysed in this study is included in the manuscript and in the
537 supplementary data.

538 REFERENCES

- 539 1. M. Zajac, E. Dreano, A. Edwards, G. Planelles, I. Sermet-gaudelus, Airway surface liquid pH
540 regulation in airway epithelium current understandings and gaps in knowledge. *Int. J. Mol.*
541 *Sci.* **22**, 1–24 (2021).
- 542 2. C. B. Morrison, *et al.*, Treatment of cystic fibrosis airway cells with CFTR modulators
543 reverses aberrant mucus properties via hydration . *Eur. Respir. J.*, 2100185 (2021).
- 544 3. A. M. A. M. Cantin, *et al.*, Cystic fibrosis transmembrane conductance regulator function is
545 suppressed in cigarette smokers. *Am. J. Respir. Crit. Care Med.* **173**, 1139–1144 (2006).
- 546 4. V. Saint-Criq, M. A. Gray, Role of CFTR in epithelial physiology. *Cell. Mol. Life Sci.* **74**, 93–115
547 (2017).
- 548 5. M. J. Hoegger, *et al.*, Impaired mucus detachment disrupts mucociliary transport in a piglet
549 model of cystic fibrosis. *Science (80-.)*. **345**, 818–822 (2014).
- 550 6. A. A. Pezzulo, *et al.*, Reduced airway surface pH impairs bacterial killing in the porcine cystic
551 fibrosis lung. *Nature* **487**, 109–113 (2012).
- 552 7. V. S. Shah, *et al.*, Airway acidification initiates host defense abnormalities in cystic fibrosis
553 mice. *Science (80-.)*. **351**, 503–507 (2016).
- 554 8. A. L. Garland, *et al.*, Molecular basis for pH-dependent mucosal dehydration in cystic
555 fibrosis airways. *Proc. Natl. Acad. Sci. U. S. A.* (2013)
556 <https://doi.org/10.1073/pnas.1311999110>.
- 557 9. A. Schultz, *et al.*, Airway surface liquid pH is not acidic in children with cystic fibrosis. *Nat.*
558 *Commun.* (2017) <https://doi.org/10.1038/s41467-017-00532-5>.

- 559 10. M. Stigliani, *et al.*, Rheological Properties of Cystic Fibrosis Bronchial Secretion and in Vitro
560 Drug Permeation Study: The Effect of Sodium Bicarbonate. *J. Aerosol Med. Pulm. Drug*
561 *Deliv.* **29**, 337–345 (2016).
- 562 11. D. Kim, *et al.*, Large pH oscillations promote host defense against human airways infection.
563 *J. Exp. Med.* **218** (2021).
- 564 12. Y. Han, A. M. Shewan, P. Thorn, HCO₃⁻ transport through anoctamin/transmembrane
565 protein ANO1/TMEM16A in pancreatic acinar cells regulates luminal pH. *J. Biol. Chem.* **291**,
566 20345–20352 (2016).
- 567 13. J. H. Poulsen, H. Fischer, B. Illek, T. E. Machen, Bicarbonate conductance and pH regulatory
568 capability of cystic fibrosis transmembrane conductance regulator. *Proc. Natl. Acad. Sci. U.*
569 *S. A.* **91**, 5340–5344 (1994).
- 570 14. D. Kim, *et al.*, Pendrin mediates bicarbonate secretion and enhances cystic fibrosis
571 transmembrane conductance regulator function in airway surface epithelia. *Am. J. Respir.*
572 *Cell Mol. Biol.* **60**, 705–716 (2019).
- 573 15. T. Rehman, *et al.*, TNF α and IL-17 Alkalinize Airway Surface Liquid through CFTR and
574 Pendrin. *Am. J. Physiol. Physiol.* (2020) <https://doi.org/10.1152/ajpcell.00112.2020>.
- 575 16. J. P. Garnett, *et al.*, Novel role for pendrin in orchestrating bicarbonate secretion in cystic
576 fibrosis transmembrane conductance regulator (CFTR)-expressing airway serous cells. *J.*
577 *Biol. Chem.* **286**, 41069–41082 (2011).
- 578 17. V. Saint-Criq, *et al.*, Choice of Differentiation Media Significantly Impacts Cell Lineage and
579 Response to CFTR Modulators in Fully Differentiated Primary Cultures of Cystic Fibrosis
580 Human Airway Epithelial Cells. *Cells* **9**, 2137 (2020).

- 581 18. M. D. Parker, W. F. Boron, The divergence, actions, roles, and relatives of sodium-coupled
582 bicarbonate transporters. *Physiol. Rev.* **93**, 803–959 (2013).
- 583 19. J. J. Gildea, *et al.*, The sodium-bicarbonate cotransporter NBCE2 (slc4a5) expressed in
584 human renal proximal tubules shows increased apical expression under high-salt
585 conditions. *Am. J. Physiol. - Regul. Integr. Comp. Physiol.* **309**, R1447–R1459 (2015).
- 586 20. N. Abuladze, *et al.*, Axial heterogeneity of sodium-bicarbonate cotransporter expression in
587 the rabbit proximal tubule. *Am. J. Physiol. Ren. Physiol.* **274**, F628–F633 (1998).
- 588 21. S. M. Theparambil, Z. Naoshin, A. Thyssen, J. W. Deitmer, Reversed electrogenic sodium
589 bicarbonate cotransporter 1 is the major acid loader during recovery from cytosolic
590 alkalosis in mouse cortical astrocytes. *J. Physiol.* **593**, 3533–3547 (2015).
- 591 22. L. Delpiano, *et al.*, Esomeprazole increases airway surface liquid pH in primary cystic fibrosis
592 epithelial cells. *Front. Pharmacol.* **9**, 1–15 (2018).
- 593 23. V. Saint-Criq, *et al.*, Real-time, semi-automated fluorescent measurement of the airway
594 surface liquid pH of primary human airway epithelial cells. *J. Vis. Exp.* **148** (2019).
- 595 24. P. Anagnostopoulou, *et al.*, SLC26A9-mediated chloride secretion prevents mucus
596 obstruction in airway inflammation. *J. Clin. Invest.* **122**, 3629–3634 (2012).
- 597 25. G. Gorrieri, *et al.*, Goblet Cell Hyperplasia Requires High Bicarbonate Transport to Support
598 Mucin Release. *Sci. Rep.* (2016) <https://doi.org/10.1038/srep36016>.
- 599 26. H. Heidtmann, I. Ruminot, H. M. Becker, J. W. Deitmer, Inhibition of monocarboxylate
600 transporter by N-cyanosulphonamide S0859. *Eur. J. Pharmacol.* **762**, 344–349 (2015).
- 601 27. A. Schwab, *et al.*, Functional role of Na⁺-HCO₃⁻ cotransport in migration of transformed

602 renal epithelial cells. *J. Physiol.* **568**, 445–458 (2005).

603 28. F. F. T. Ch'en, F. C. Villafuerte, P. Swietach, P. M. Cobden, R. D. Vaughan-Jones, S0859, an
604 N-cyanosulphonamide inhibitor of sodium-bicarbonate cotransport in the heart. *Br. J.*
605 *Pharmacol.* **153**, 972–982 (2008).

606 29. J. J. Smith, M. J. Welsh, cAMP stimulates bicarbonate secretion across normal, but not
607 cystic fibrosis airway epithelia. *J. Clin. Invest.* **89**, 1148–1153 (1992).

608 30. D. C. Devor, *et al.*, Bicarbonate and chloride secretion in Calu-3 human airway epithelial
609 cells. *J. Gen. Physiol.* **113**, 743–760 (1999).

610 31. I. Kurtz, NBCe1 as a model carrier for understanding the structure-function properties of
611 Na⁺-coupled SLC4 transporters in health and disease. *Pflugers Arch. Eur. J. Physiol.* **466**,
612 1501–1516 (2014).

613 32. A. K. M. Shamsuddin, P. M. Quinton, Concurrent absorption and secretion of airway surface
614 liquids and bicarbonate secretion in human bronchioles. *Am. J. Physiol. - Lung Cell. Mol.*
615 *Physiol.* **316**, L953–L960 (2019).

616 33. J. L. Kreindler, K. W. Peters, R. A. Frizzell, R. J. Bridges, Identification and membrane
617 localization of electrogenic sodium bicarbonate cotransporters in Calu-3 cells. *Biochim.*
618 *Biophys. Acta - Mol. Basis Dis.* **1762**, 704–710 (2006).

619 34. P. Scudieri, *et al.*, Association of TMEM16A chloride channel overexpression with airway
620 goblet cell metaplasia. *J. Physiol.* **590**, 6141–6155 (2012).

621 35. S. M. Kreda, *et al.*, Characterization of wild-type and Δ F508 cystic fibrosis transmembrane
622 regulator in human respiratory epithelia. *Mol. Biol. Cell* **16**, 2154–2167 (2005).

- 623 36. D. Yang, *et al.*, IRBIT coordinates epithelial fluid and HCO₃⁻ secretion by stimulating the
624 transporters pNBC1 and CFTR in the murine pancreatic duct. *J. Clin. Invest.* **119**, 193–202
625 (2009).
- 626 37. K. Shirakabe, *et al.*, IRBIT, an inositol 1,4,5-trisphosphate receptor-binding protein,
627 specifically binds to and activates pancreas-type Na⁺/HCO₃⁻ cotransporter 1 (pNBC1).
628 *Proc. Natl. Acad. Sci. U. S. A.* **103**, 9542–9547 (2006).
- 629 38. D. T. Montoro, *et al.*, A revised airway epithelial hierarchy includes CFTR-expressing
630 ionocytes. *Nature* **560**, 319–324 (2018).
- 631 39. L. W. Plasschaert, *et al.*, A single-cell atlas of the airway epithelium reveals the CFTR-rich
632 pulmonary ionocyte. *Nature* **560**, 377–381 (2018).
- 633 40. J. F. Engelhardt, M. Zepeda, J. A. Cohn, J. R. Yankaskas, J. M. Wilson, Expression of the cystic
634 fibrosis gene in adult human lung. *J. Clin. Invest.* **93**, 737–749 (1994).
- 635 41. K. Okuda, *et al.*, Secretory cells dominate airway CFTR expression and function in human
636 airway superficial epithelia. *Am. J. Respir. Crit. Care Med.* **203**, 1275–1289 (2021).
- 637 42. A. Hahn, *et al.*, Expression and function of Anoctamin 1/TMEM16A calcium-activated
638 chloride channels in airways of in vivo mouse models for cystic fibrosis research. *Pflugers*
639 *Arch. Eur. J. Physiol.* **470**, 1335–1348 (2018).
- 640 43. A. Hahn, *et al.*, Cellular distribution and function of ion channels involved in transport
641 processes in rat tracheal epithelium. *Physiol. Rep.* **5**, 1–14 (2017).
- 642 44. C. E. Jia, D. Jiang, H. Dai, F. Xiao, C. Wang, Pendrin, an anion exchanger on lung epithelial
643 cells, could be a novel target for lipopolysaccharide-induced acute lung injury mice. *Am. J.*

644 *Transl. Res.* **8**, 981–992 (2016).

645 45. R. Ratcliff, *et al.*, Production of a severe cystic fibrosis mutation in mice by gene targeting.
646 *Nat. Genet.* **4**, 35–41 (1993).

647 46. J. N. Snouwaert, *et al.*, An Animal Model for Cystic Fibrosis Made by Gene Targeting.
648 *Science (80-.)*. **257**, 1083–1088 (1992).

649 47. J. R. Rock, *et al.*, Transmembrane protein 16A (TMEM16A) is a Ca²⁺ -regulated Cl⁻ secretory
650 channel in mouse airways. *J. Biol. Chem.* (2009) <https://doi.org/10.1074/jbc.C109.000869>.

651 48. B. R. Grubb, A. J. Pace, E. Lee, B. H. Koller, R. C. Boucher, Alterations in airway ion transport
652 in NKCC1-deficient mice. *Am. J. Physiol. - Cell Physiol.* **281**, 615–623 (2001).

653 49. X. X. Tang, *et al.*, Acidic pH increases airway surface liquid viscosity in cystic fibrosis. *J. Clin.*
654 *Invest.* **126**, 879–891 (2016).

655 50. L. Ferrera, V. Capurro, L. Delpiano, A. Gianotti, O. Moran, The application of bicarbonate
656 recovers the chemical-physical properties of airway surface liquid in cystic fibrosis epithelia
657 models. *Biology (Basel)*. **10** (2021).

658 51. J. Simonin, *et al.*, Airway surface liquid acidification initiates host defense abnormalities in
659 Cystic Fibrosis. *Sci. Rep.* **9**, 1–11 (2019).

660 52. S. E. Birket, *et al.*, Development of an airway mucus defect in the cystic fibrosis rat. *JCI*
661 *insight* **3** (2018).

662 53. J. L. Cooper, P. M. Quinton, S. T. Ballard, Mucociliary transport in porcine trachea:
663 Differential effects of inhibiting chloride and bicarbonate secretion. *Am. J. Physiol. - Lung*
664 *Cell. Mol. Physiol.* **304**, 184–190 (2013).

- 665 54. L. R. Gawenis, *et al.*, Colonic anion secretory defects and metabolic acidosis in mice lacking
666 the NBC1 Na⁺/HCO₃⁻ cotransporter. *J. Biol. Chem.* (2007)
667 <https://doi.org/10.1074/jbc.M607041200>.
- 668 55. Y. F. Lo, *et al.*, Severe metabolic acidosis causes early lethality in NBC1 W516X knock-in
669 mice as a model of human isolated proximal renal tubular acidosis. *Kidney Int.* **79**, 730–741
670 (2011).
- 671 56. S. M. Theparambil, I. Ruminot, H. P. Schneider, G. E. Shull, J. W. Deitmer, The electrogenic
672 sodium bicarbonate cotransporter NBCe1 is a high-affinity bicarbonate carrier in cortical
673 astrocytes. *J. Neurosci.* **34**, 1148–1157 (2014).
- 674 57. N. Takahashi, *et al.*, Uncompensated polyuria in a mouse model of Bartter's syndrome.
675 *Proc. Natl. Acad. Sci. U. S. A.* **97**, 5434–5439 (2000).
- 676 58. E. E. Salerno, *et al.*, Extrarenal signs of proximal renal tubular acidosis persist in
677 nonacidemic Nbce1b/c-Null mice. *J. Am. Soc. Nephrol.* **30**, 979–989 (2019).
- 678 59. H. W. Lee, *et al.*, NBCe1-a regulates proximal tubule ammonia metabolism under basal
679 conditions and in response to metabolic acidosis. *J. Am. Soc. Nephrol.* **29**, 1182–1197
680 (2018).
- 681 60. R. Rozmahel, *et al.*, Modulation of disease severity in cystic fibrosis transmembrane
682 conductance regulator deficient mice by a secondary genetic factor. *Nat. Genet.* **12**, 280–
683 287 (1996).
- 684 61. G. R. Cutting, Modifier genes in Mendelian disorders: the example of cystic fibrosis.
685 *Ann. N. Y. Acad. Sci.* **1214**, 57–69 (2010).

62. A. R. Philp, *et al.*, Kcnn4 is a modifier gene of intestinal cystic fibrosis preventing lethality in the CFTR-F508del mouse. *Sci. Rep.* **8**, 9328 (2018).
63. F. A. Suprynowicz, *et al.*, Conditionally reprogrammed cells represent a stem-like state of adult epithelial cells. *Proc. Natl. Acad. Sci. U. S. A.* **109**, 20035–20040 (2012).
64. S. H. Randell, M. L. Fulcher, W. K. O’Neal, J. C. Olsen, “Primary Epithelial Cell Models for Cystic Fibrosis Research.” in *Cystic Fibrosis*, (Springer International Publishing, 2011), pp. 285–210.
65. M. J. Turner, *et al.*, Hypercapnia modulates cAMP signalling and cystic fibrosis transmembrane conductance regulator-dependent anion and fluid secretion in airway epithelia. *J. Physiol.* **594**, 1643–1661 (2016).
66. V. Saint-Criq, S. H. Kim, J. A. Katzenellenbogen, B. J. Harvey, Non-genomic estrogen regulation of ion transport and airway surface liquid dynamics in cystic fibrosis bronchial epithelium. *PLoS One* **8**, e78593 (2013).
67. G. Vega, *et al.*, Lack of Kcnn4 improves mucociliary clearance in muco-obstructive lung disease. *JCI Insight* **5**, 140076 (2020).
68. A. Gianotti, *et al.*, Pharmacological analysis of epithelial chloride secretion mechanisms in adult murine airways. *Eur. J. Pharmacol.* **781**, 100–108 (2016).
69. S. M. Theparambil, J. W. Deitmer, High effective cytosolic H⁺ buffering in mouse cortical astrocytes attributable to fast bicarbonate transport. *Glia* **63**, 1581–1594 (2015).

707 ACKNOWLEDGMENTS

708 This work was supported by two CF Trust Strategic Research Centre grants (SRC003 and SRC013)
709 and a Medical Research Council (MRC) Confidence in Concept grant (MC_PC_15030) and
710 FONDECYT 1221257 (C.A.F.). The Centro de Estudios Científicos (CECs) was funded by the Base
711 Financing Programme of CONICYT, Chile. Cells from Dr. Randell were supported by Cystic Fibrosis
712 Foundation grant (BOUCHE15R0) and NIH grant (P30DK065988). We would like to acknowledge
713 Drs. Scott H. Randell and Leslie Fulcher (Marsico Lung Institute, The University of North Carolina at
714 Chapel Hill, United States) for providing human primary airway epithelial cells from the UNC CF
715 Center Tissue Procurement and Cell Culture Core. Git Chung for human kidney RNA sample.

716

717

Figure 1. Basal bicarbonate secretion requires SLC4A4 activity in primary hAECs. Mean traces (+ standard error of the mean) of I_{sc} in (A) Cl^- free solution (n=14) and (D) HCO_3^- free solution (n=10) of primary hAECs cultures (dotted lines represent the time of addition of drugs). Summary of S0859-induced changes in I_{sc} in the presence (B) or absence (E) of HCO_3^- in primary hAECs cultures and Fsk-induced HCO_3^- secretion (C) in Cl^- free buffer (on panels B, C and E, each dot represents an independent experiment; means \pm sem are shown next to the individual data; respectively n=17, n=14 and n=11 independent experiments using cells from N=3 donors; two-tailed, paired t-test). (F) Representative pH_i trace of primary hAECs bathed first in bilateral HCO_3^- KRB (gassed with 5% CO_2) then bilateral Hepes buffered KRB (no HCO_3^- , no CO_2) and then bilateral HCO_3^- KRB (gassed with 5% CO_2). CO_2 removal and re-introduction is marked by a transient increase and decrease in pH_i respectively. (G) Representative trace of pH_i recovery after CO_2 -induced acidification in the absence of basolateral HCO_3^- . (H) Representative trace of pH_i recovery after CO_2 -induced acidification in the absence of basolateral Na^+ and HCO_3^- . (I) Summary of the magnitude of CO_2 -induced acidification (bilateral bicarbonate, n=7, apical bicarbonate n=14, unpaired t-test, bars represent mean \pm standard deviation (S.D.)). (J) Mean percentage of pH_i recovery after perfusion of the different solutions (Bilateral Bicarbonate, n=7; Apical Bicarbonate, n=14; Bilateral Bicarbonate after Apical Bicarbonate $^-$, n=5; Na^+ -free buffer, n=8; Bilateral Bicarbonate after Na^+ -free buffer, n=8; One-way ANOVA with Holm-Sidak correction for multiple comparison tests, bar graph represents mean \pm S.D.). (K) Representative trace of intracellular pH measurements showing recovery from CO_2 -induced acidification in the presence (red line) or absence (blue line) of NBC inhibitor S0859. (L) Summary of rates of recovery from CO_2 -induced acidification in the presence of NHE inhibitor (Dimethyl Amiloride, DMA, 100 μ M) and in the presence (red bar) or absence (blue bar) of S0859 (30 μ M), (n = 3, paired t-test; bars represent mean \pm S.D.).

Figure 1-figure supplement 1. Expression of SLC4A family members of bicarbonate transporters in differentiated primary human airway epithelial cells. Amplicons for SLC4A4 (A,E), SLC4A5 (B), SLC4A7 (C), SLC4A8 (D) and SLC4A10 (F) were amplified from differentiated human airway epithelial cells from 3 donors. Pancreatic and renal isoforms of SLC4A4 were detected in the airway epithelial cell line Calu-3 (lane 2, left panelsA-D) and human kidney (lane2, right panelsE-F). Normalised gene counts were extracted from previously published RNA-seq data (Saint-Criq et al Cells 2020) to confirm the expression pattern of SLC4A family members and other HCO₃-transporters such as Bestrophins (G). Each symbol represents cells from an individual donor and bars represent means \pm SD. FIGURE 2

Figure 2. S0859 decreases resting ASL pH in primary human airway epithelial cells (hAECs), by blocking basolateral SLC4A4. (A) Mean (+S.E.M.) trace of ASL pH recordings. ASL pH was measured under resting conditions for 1.5hr before S0859 (30 μ M) was added basolaterally. (B) Mean resting ASL pH before (black circles) and after (blue circles) addition of basolateral S0859 (n=9 independent experiments performed on epithelial cells from N=3 donors; paired t-test). (C) Mean (+SEM) traces of ASL pH from hAECs pre-treated for 3 h with vehicle control (DMSO, black trace) or S0859 (30 μ M, basolateral, blue trace). (D) Mean Forskolin (Fsk)-induced changes in ASL pH in hAECs treated with DMSO (black circles) or S0859 (blue circles) (n=9 independent experiments performed on epithelial cells from N=3 donors; paired t-test). (E) Mean (+SEM) traces of ASL pH from hAECs treated with Fsk for 2.5 h and then S0859. (F) Mean Fsk-stimulated ASL pH before (black circles) and after (blue circles) addition of basolateral S0859 (n=9 independent experiments performed on epithelial cells from N=3 donors; paired t-test). (G-H) SLC4A4 locates in the basolateral membrane of acetylated tubulin (Ac-tubulin) positive human airway epithelial cells. (I-J) correspond to negative controls for anti-SLC4A4 omitted antibody. Representative images of 3 different samples. Bar 20 μ M.

FIGURE 3. Basal and inducible bicarbonate secretion relies in SLC4A4 activity in mouse tracheal epithelium. Representative traces of I_{SC} in (A) bicarbonate and (B) HEPES buffer of freshly excised mouse tracheas. (C) Summary of ΔI_{SC} values for amiloride-sensitive Na^+ absorption, IBMX+Fsk-induced and A.U.C. I_{SC} UTP-induced anion secretion in mouse tracheas; n=6 for each condition; Mann-Whitney Rank Sum Test. Representative I_{SC} traces of S0859 effect on unstimulated tracheas in (D) bicarbonate and (E) HEPES buffer. (F) Summary of ΔI_{SC} values for S0859 effect, n= 5 for each condition; Mann-Whitney Rank Sum Test. Representative I_{SC} traces for UTP-induced anion secretion in absence (G and I) or presence (H and J) of 30 μM S0859 in buffer bicarbonate (G and H) or HEPES (I and J). All in the presence of 10 μM amiloride. (K) Summary of experiments as presented in G-J; n=5 but HEPES+S0859 n=6; ANOVA on Ranks. Bars are mean \pm S.E.M. (L) Average response of determination of pH_i in epithelial cells isolated from wild type mouse trachea and loaded with BCECF that were stimulated with 100 μM UTP and switched to 12.5 mM bicarbonate buffered solution. Experiments performed in bicarbonate buffer in blue and HEPES in red. (M) Summary of ΔpH_i from experiments as those in (L) including a data set of cells maintained in HEPES buffer; Middle line of the box plot indicates the median; n=15 cells from 4 different mice, n=11 cells, 3 different mice and n=13 cells, 3 different mice respectively; ANOVA on Ranks.

Figure 3 –figure supplement 1. Expression of SLC4 family members of bicarbonate transporters
in mouse airway epithelial cells. Amplicons for (A) *Slc4a4*, (B) *Slc4a5*, (C) *Slc4a7*, (D) *Slc4a8* and (E) *Slc4a10* were amplified from 4 samples of airway epithelial cells isolated from 4 different animals.
(F) Isoforms of *Slc4a4* were detected in airway epithelial cells (lane 2) and mouse kidney (lane3).
Lane 4 corresponds to negative RT-PCR control. Image representative of 4 samples tested.

Figure 3-figure supplement 2. (A) Representative trace of S0859 (30 μ M) effect on IBMX+Fsk-induced anion secretion, (B) individual experiments showing I_{sc} changes and (C) summary of ΔI_{sc} values for IBMX+Fsk-induced anion secretion and S0859. (D) Representative trace of S0859 (30) effect on IBMX+Fsk-induced anions secretion after inhibition of apical chloride secretion by addition of CaCCinhA01 (30 μ M), (E) individual experiments showing I_{sc} changes and (F) summary of ΔI_{sc} values for experiments in (D). (G) UTP-induced intracellular acidification in the presence of 30 μ M S0859 in bicarbonate buffer. (H) Summary of experiments showing $\Delta pH_{[i]}$; n=14 cells from 4 different mice; Mann-Whitney Rank Sum Test.

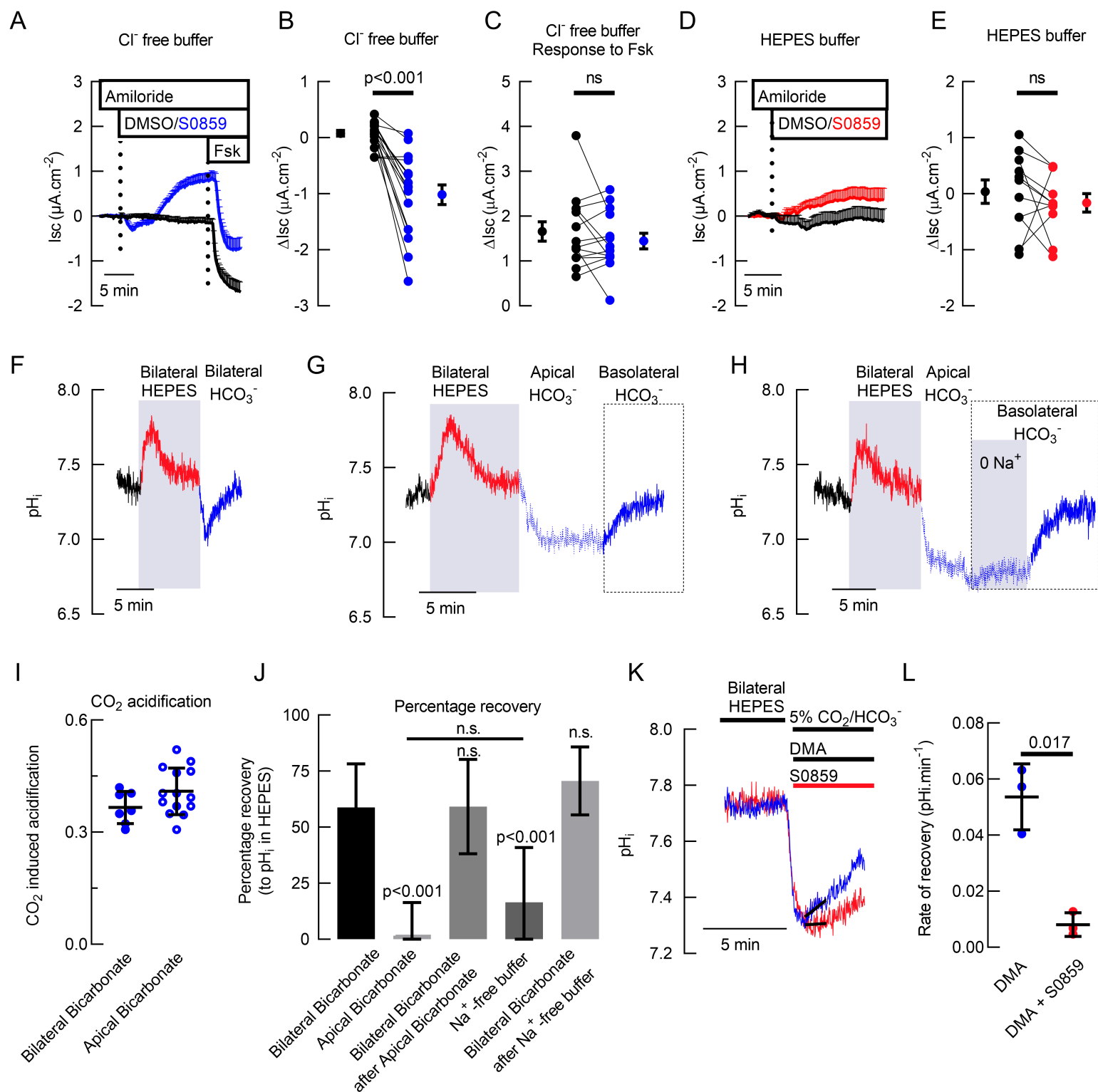
FIGURE 4. The *Slc4a4*^{-/-} bear signs of muco-obstructive airway disease. (A) Ventral view of Alcian blue stained tracheas of 17 days old mice. Red arrow heads show incomplete cartilage rings in the *Slc4a4*^{-/-} mouse; representative image of 3 animals per genotype. (B) SLC4A4 staining of epithelial cells is absent in the *Slc4a4*^{-/-} lung tissues; representative images of 3 different animals per genotype. (C) Epithelial SLC4A4 co-localizes with CCSP; representative images of 3 different animals. (D) Mucin staining showing mucus adhered to the epithelial surface and epithelial damage (red arrow heads); representative images of 5 animals per genotype. (E) Summary of R_{te} values for wild type and *Slc4a4*^{-/-} tracheas; dashed line indicates $50 \Omega\text{cm}^{-2}$; n= 8 for wild types and n=6 for *Slc4a4*^{-/-} tracheas. (F) Representative traces of pH_i in airway cells from wild type (blue) and *Slc4a4*^{-/-} (red) animals and (G) summary of UTP-induced ΔpH_i including mean \pm S.E.M. and individual cells; n=8 cells for wild type and n=6 cells for *Slc4a4*^{-/-}, 3 different animals per genotype; Mann-Whitney Rank Sum Test. (H) Beads tracking of MCC experiments for wild type and *Slc4a4*^{-/-} tracheas bathed with basolateral bicarbonate or HEPES buffer. Radius of the polar plots is 50 μm . Summary of MCC experiments for (I) speed, (J) total distance covered by beads. Bars indicate mean \pm S.E.M.; n=5 for each genotype in bicarbonate buffer and n=4 for each genotype in HEPES buffer; ANOVA on ranks.

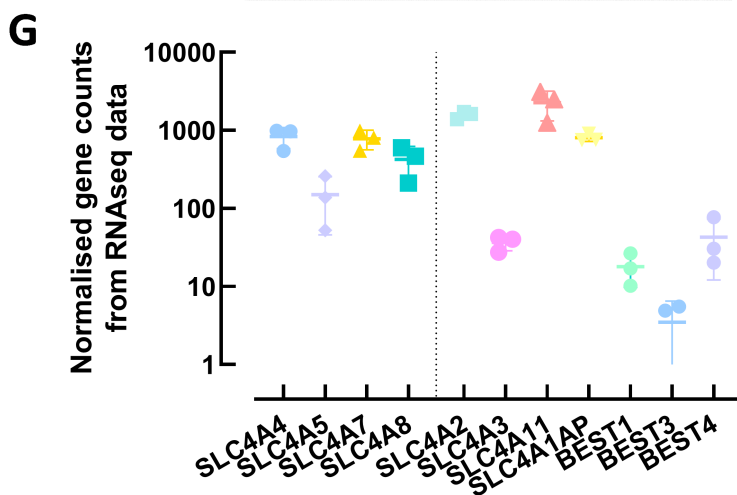
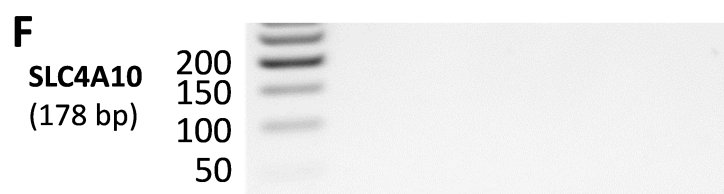
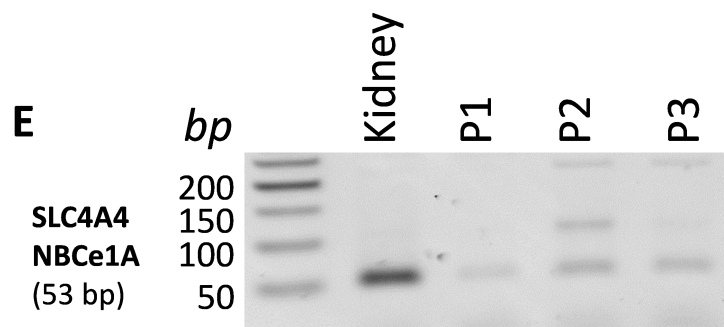
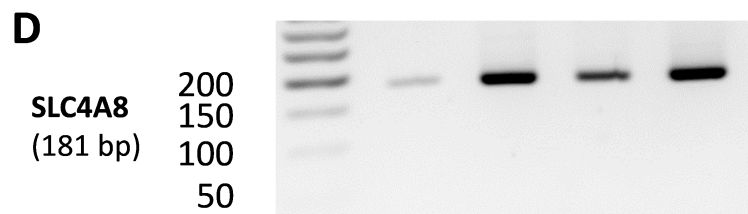
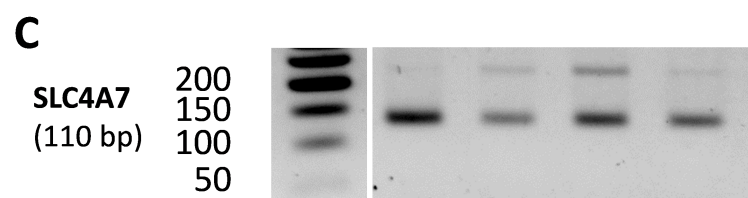
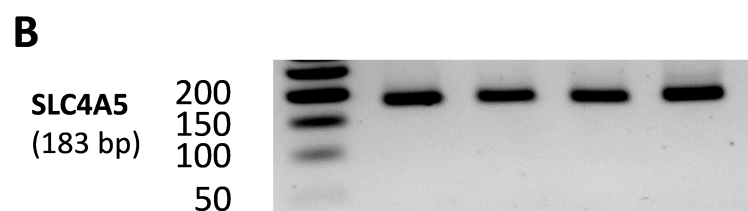
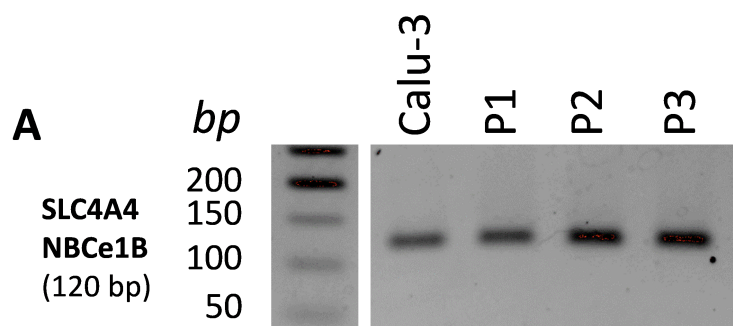
Figure 4-figure supplement 1. *Slc4a4* silencing produces early lethality, weight loss, mucus accumulation and reduced intracellular pH. (A) Kaplan-Meier curves showing survival for *Slc4a4*^{-/-} in the C57Bl6/J (B6; red line) or hybrid background (Hyb; blue line). Log-Rank test; n=12 and 16 per group. (B) Weight gain curves for control and *Slc4a4*^{-/-} (KO) mice in B6 and Hyb backgrounds; n=5 for each group but for KO B6 that due to increased lethality group is reduced as indicated in the numbers on top of last 2 records. (C) Epithelial SLC4A4 co-localizes with CCSP protein in bronchi and bronchioles; representative images of 3 animals per genotype. (D-I) PAS staining of mucus in trachea (D-E), bronchi (F-H) and bronchiole (I). Red arrows indicate areas of epithelial damage. Images are representative of 5 different animals per genotype. (J) Summary of $\Delta \text{pH}_{\text{ij}}$ post-UTP including mean \pm S.E.M. and individual cells; n=8 cells for wild type and n=6 cells for *Slc4a4*^{-/-}, 3 different animals per genotype; Mann-Whitney Rank Sum Test.

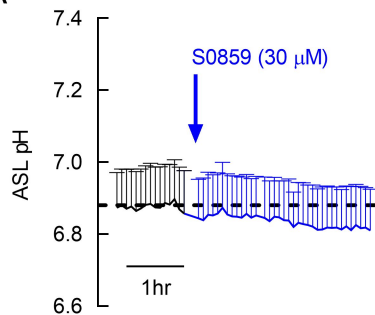
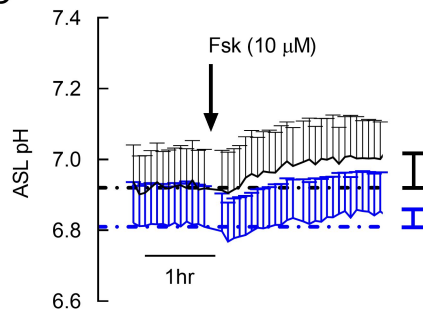
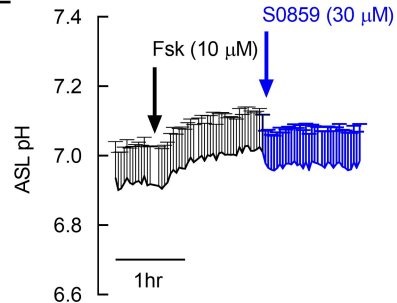
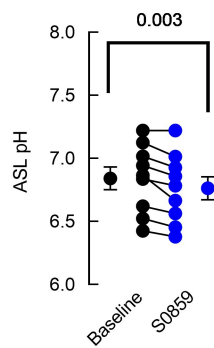
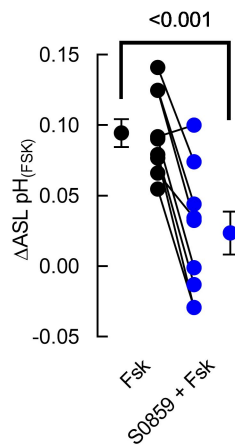
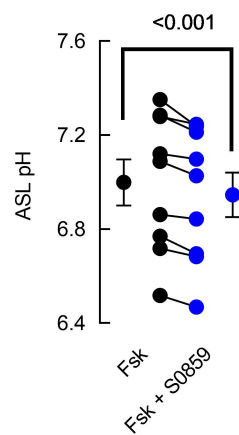
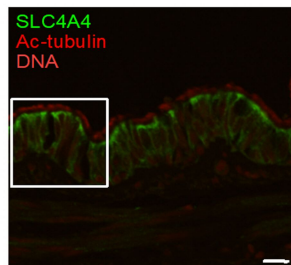
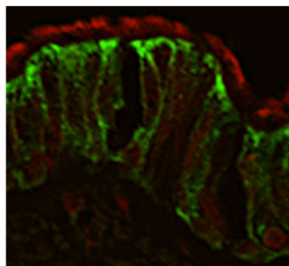
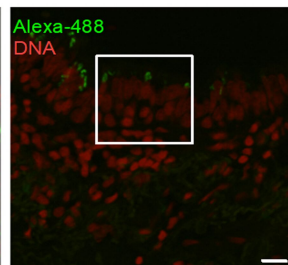
Figure 1-figure supplement 1 - Source data 1
Figure 3 -figure supplement 1- Source data 1

Supplementary File 1: Primers for hBECs

Supplementary File 2: Primers for mouse





A**C****E****B****D****F****G****H****I****J**